Luminescence Spectroscopy and Near-Infrared to Visible Upconversion of Nanocrystalline $Gd_3Ga_5O_{12}$:Er^{3+}

Fiorenzo Vetrone, John-Christopher Boyer, and John A. Capobianco*

Department of Chemistry and Biochemistry, Concordia University, 1455 de Maisonneuve Blvd. W, Montreal, QC, H3G-1M8, Canada

Adolfo Speghini and Marco Bettinelli

Dipartimento Scientifico e Tecnologico, Università di Verona, and INSTM, UdR Verona, Ca' Vignal, Strada Le Grazie 15, I-37134 Verona, Italy

Received: April 11, 2003; In Final Form: June 27, 2003

The near-infrared to visible upconversion properties of nanocrystalline $Gd_3Ga_5O_{12}$:Er^{3+} (1 and 5%) were studied following excitation of the $^4I_{9/2}$ exited state with 800 nm radiation. Intense green and red emissions were observed from the ($^2H_{11/2}$, $^4S_{3/2}$) → $^4I_{15/2}$ and $^4F_{9/2}$ → $^4I_{15/2}$ transitions, respectively. The upconverted decay times in the 1% sample were identical compared to those obtained with 488 nm excitation, indicating that ESA was responsible for populating the upper emitting states. However, as the Er^{3+} concentration was increased to 5%, the upconverted decay times were lengthened and deviated from exponentiality, indicating the presence of energy transfer upconversion. In addition, an enhancement of the red ($^4F_{9/2}$ → $^4I_{15/2}$) upconversion emission was observed in the 5% sample and occurred via an energy transfer process of the type ($^4I_{9/2}$, $^4I_{11/2}$) → ($^4I_{13/2}$, $^4F_{9/2}$).

1. Introduction

In recent years, the field of luminescence and display materials has undergone a revival of sorts with the evolution to nanosized luminescing particles. A wide range of nanocrystalline materials, from semiconductors to rare-earth-doped insulators, have been actively studied since the physical and optical properties have been shown to change remarkably as the size of the particle is reduced to the nanometer regime.[1] Many of the initial studies on nanocrystalline insulators focused on rare-earth-doped Y_2O_3, due to its favorable physical properties and ease of synthesis in its nanocrystalline form. It was with Y_2O_3:RE^{3+} nanocrystals that the particle-size-dependent phenomena were first observed in insulating materials.[2]

Recently, studies on the luminescent properties of more complex rare-earth-doped nanocrystalline insulating materials such as vanadates,[3,4] titanates,[5] molybdates,[6] and fluorides,[7] as examples, have appeared in the literature. Other than yttrium aluminum garnet (YAG, $Y_3Al_5O_{12}$),[8−11] very little work on rare-earth-doped nanocrystalline garnets has been done. Furthermore, the work that has been done on the garnet nanocrystals has focused on the Stokes emission whereas the anti-Stokes (or upconversion) properties have been largely overlooked. The phenomenon of upconversion has been studied extensively over the past few years and it is an important process for the generation of visible light from near-infrared radiation. It is essentially defined as the optical illumination of a rare-earth or transition-metal ion doped material, which produces a population in an excited state, whose energy exceeds that of the pump photon.[12,13] Rare-earth ions such as Pr^{3+}, Nd^{3+}, Sm^{3+}, Dy^{3+}, Ho^{3+}, Er^{3+}, and Tm^{3+} have all demonstrated upconversion and are particularly suited to undergo this process as they possess several excited states with long lifetimes that are well matched to the emission wavelengths of several efficient pump laser sources.

The garnets make up one of the most important groups of hosts for laser active centers, especially for trivalent rare earth ions. They are attractive from a physical standpoint as they are transparent from the UV to the mid-IR and thus they can be used as window material for a variety of lamps. Furthermore, they have high thermal conductivity, hardness, and chemical stability.[14] Without doubt, the best known garnet is $Y_3Al_5O_{12}$ (YAG, yttrium aluminum garnet) and when doped with Nd^{3+} constitutes one of the most widely used laser active material ($\lambda_{em} = 1.06\ \mu m$). However, the GGG:$Nd^{3+}$ ($Gd_3Ga_5O_{12}$:Nd^{3+}) material possesses several advantages over the YAG:Nd^{3+} single crystals as its melting temperature is lower, growth rate is faster, and it is possible to obtain crystals with large dimensions, high optical quality, and higher concentration of activator ions.[15] Also, GGG ($n_{GGG} = 1.965$) has a higher index of refraction than YAG ($n_{YAG} = 1.816$),[16] which is beneficial for radiative transitions in RE^{3+} ions.

The overall crystal structure of the garnets is cubic and belongs to the O^{10}_h ($Ia3d$) space group with eight equivalent gadolinium sites per elementary unit cell and having a lattice parameter of approximately 12 Å.[17] Their molecular formula can be expressed as $A_3B_2C_3O_{12}$, where B and C may be the same atoms ($Gd_3Ga_2Ga_3O_{12}$). The garnet lattice possesses three crystallographically distinct cation sites (c, a, and d, see Figure 1) available for dopant ion substitution.[18] In the c-site which has D_2 symmetry, the A ions are surrounded by a distorted dodecahedron of eight O^{2-} ions while the B ions in the a-site of C_{3i} symmetry are surrounded by a trigonally distorted octahedron of O^{2-} ions. Finally in the d-site, which has S_4 site

* Author to whom correspondence should be addressed. Tel: +1-514-848-3350. Fax: +1-514-848-2868. E-mail: capo@vax2.concordia.ca.

10.1021/jp030434r CCC: $25.00
Published on Web 09/06/2003

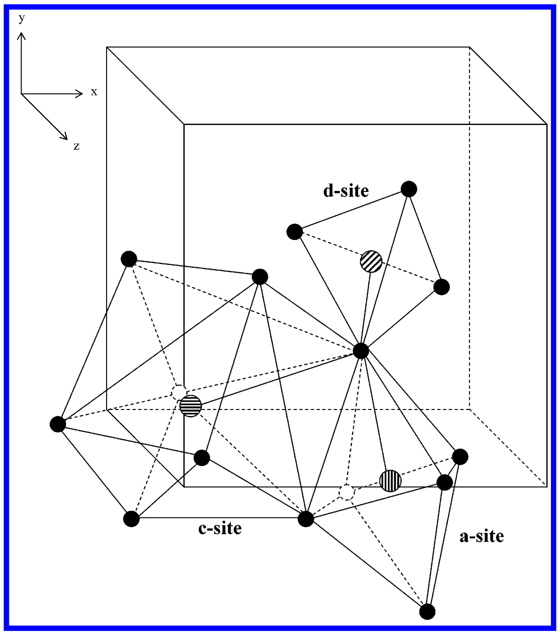

Figure 1. Schematic representation of the $Gd_3Ga_5O_{12}$ unit cell showing the c, a, and d sites.

symmetry, the C ions are surrounded by an O^{2-} tetrahedron. Due to ionic size considerations in the GGG lattice, the Er^{3+} ions will predominantly enter the dodecahedral c-sites by replacing the Gd^{3+} and therefore possess D_2 symmetry. On the other hand, the transition metal ions will substitute the ions in the octahedral and/or tetrahedral sites of the garnet lattice.[14]

Upconverted emission has been previously demonstrated in GGG single crystals doped with erbium following infrared excitation. For example, green emission was observed in GGG:Er^{3+} following excitation into the $^4I_{11/2}$ state [19] and was also observed in GGG doped with Er^{3+} and sensitized with Cr^{3+} following the cooperative upconversion of 2 Er^{3+} ions in the $^4I_{13/2}$ state.[20] Upconversion was also observed in gadolinium gallium garnet doped with Pr^{3+},[21] and in both Ho^{3+} [22] and Tm^{3+} [23] codoped with Yb^{3+}. However, to the best of our knowledge, upconversion in nanocrystalline GGG has not yet been reported. In this paper, we study the upconversion properties of nanocrystalline GGG doped with 1 and 5% Er^{3+} following excitation of the $^4I_{9/2}$ excited state with 800 nm. The various mechanisms responsible for populating the upper excited states are elucidated and discussed.

2. Experimental Section

Sample Preparation. $Gd_3Ga_5O_{12}$ nanocrystals doped with 1 and 5% Er^{3+} were prepared using a solution combustion (propellant) synthesis procedure, which is a novel technique capable of producing nanopowders at relatively low temperatures and in a timely manner.[24,25] This process involves the exothermic reaction between the metal nitrates (oxidizer) and an organic fuel, such as urea, glycine, or carbohydrazide. An aqueous solution containing appropriate quantities of carbohydrazide $(NH_2NH)_2CO$ (Aldrich, 98%), $Gd(NO_3)_3 \cdot 6H_2O$ (Aldrich, 99.99%), $Ga(NO_3)_3 \cdot H_2O$ (Aldrich, 99.999%), and $Er(NO_3)_3 \cdot 6H_2O$ (Aldrich, 99.9%) was prepared. A carbohydrazide-to-metal nitrate molar ratio of 2.5 was employed. The precursor solution was heated with a Bunsen flame and after the evaporation of the solvent, the auto combustion process took place with the evolution of a brown fume. After a few seconds elapsed, a very porous voluminous mass of the powder was formed. The proposed stoichiometric synthesis reaction is as follows:

$$3(1-x)Gd(NO_3)_3 + 5Ga(NO_3)_3 + 3xEr(NO_3)_3 + 3(NH_2NH)_2CO \rightarrow (Gd_{1-x}Er_x)_3Ga_5O_{12} + 24NO_2 + 6N_2 + 3CO_2 + 9H_2O$$

After combustion, the fluffy powders were fired for 1 h at 500 °C in order to decompose the residual carbohydrazide and nitrate ions. The generation of a large amount of gaseous products is an important property of the synthesis procedure as it increases the surface area of the powders; and as more gases are liberated the agglomerates are disintegrated, causing more heat to be carried from the system thereby hindering the particle growth.[9] Wide-angle powder X-ray diffraction revealed that the nanoparticles have a diameter of approximately 10 nm.

All nanocrystalline samples were kept in air without any further precaution.

Infrared Reflectance Spectroscopy. The diffuse reflectance spectra in the medium-infrared (MIR) region were measured at room temperature using a Nicolet Magna 760 FTIR spectrometer using an aluminated mirror as a reference.

Luminescence Spectroscopy. Visible emission spectra were acquired using 488 nm from a Coherent Sabre Innova, 20 W argon ion laser. Upconversion emission spectra were obtained using 800 nm from a Spectra-Physics model 3900 titanium sapphire laser pumped by the 514.5 nm line of the Coherent Sabre Innova Ar^+ laser. Emissions from nanocrystalline $Gd_3Ga_5O_{12}$:Er^{3+} were collected at $\pi/2$ from the incident beam and dispersed using a 1 m Jarrell-Ash Czerny-Turner double monochromator. The visible light exiting the monochromator was detected using a thermoelectrically cooled Hamamatsu R943-02 photomultiplier tube with a background dark count rate of less than 10 counts per second. The photomultiplied signals were processed by a Stanford Research Systems (SRS) model SR440 preamplifier, and a gated photon counter Stanford Research Systems model SR400 data acquisition system was utilized as an interface between the computer and the spectroscopic equipment. A computer using the SRS SR465 data acquisition software was used to record the signal.

The near-infrared (NIR) emission spectra were acquired using the 488 nm line of the argon ion laser and recorded with a Jarrell-Ash 3/4 meter Czerny-Turner single monochromator in second order. The signal was detected by a Northcoast EO-817P liquid nitrogen-cooled germanium detector connected to a computer-controlled Stanford Research Systems model SR510 lock-in amplifier.

All spectroscopic measurements were carried out at room temperature.

Decay Time Measurements. Decay curves were measured by modulating the 488 and 800 nm excitation wavelengths using an Stanford Research Systems SR540 optical chopper and obtained using the same data acquisition system as above.

3. Results and Discussion

Wide-angle powder X-ray diffraction has confirmed that the samples under investigation contain GGG and that no important contamination from other phases is present. The broadening of the diffraction peaks indicates that the particle sizes are in the 10 nm range. A detailed investigation of the structure and morphology of these materials is presently under way.[26]

Following the direct excitation of the $^4F_{7/2} \leftarrow {}^4I_{15/2}$ transition of the erbium ion with 488 nm, green, red, and NIR emission was observed in nanocrystalline gadolinium gallium garnet

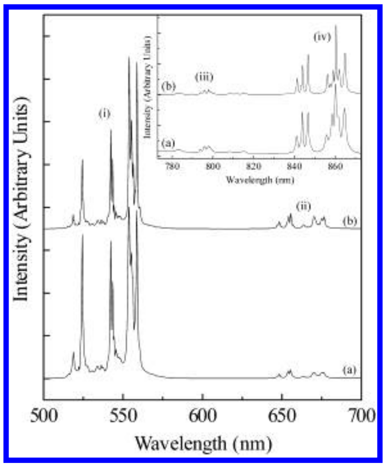

Figure 2. Emission spectrum of nanocrystalline GGG:Er^{3+} doped with (a) 1% and (b) 5% Er^{3+} following excitation with 488 nm and showing the following transitions: (i) ($^2H_{11/2}$, $^4S_{3/2}$) → $^4I_{15/2}$, (ii) $^4F_{9/2}$ → $^4I_{15/2}$. Inset: (iii) $^4I_{9/2}$ → $^4I_{15/2}$, (iv) $^4S_{3/2}$ → $^4I_{13/2}$.

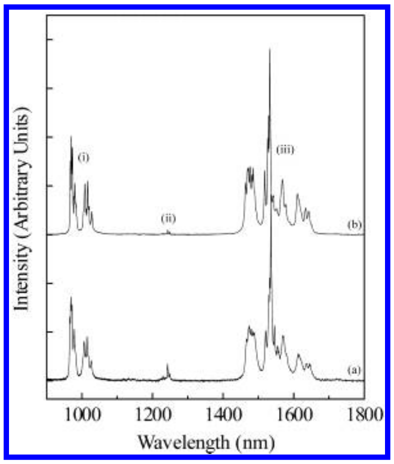

Figure 3. NIR emission spectrum of nanocrystalline GGG:Er^{3+} doped with (a) 1% and (b) 5% Er^{3+} following excitation with 488 nm and showing the following transitions: (i) $^4I_{11/2}$ → $^4I_{15/2}$, (ii) $^4S_{3/2}$ → $^4I_{11/2}$, (iii) $^4I_{13/2}$ → $^4I_{15/2}$.

doped with 1 and 5% Er^{3+} (Figure 2). Green emission was observed between 510 and 580 nm and was ascribed to the transition from the thermalized $^2H_{11/2}$, $^4S_{3/2}$ excited states to the $^4I_{15/2}$ ground state. Red emission between 630 and 700 nm was observed and attributed to the $^4F_{9/2}$ → $^4I_{15/2}$ transition. The spectra of the $^4S_{3/2}$ → $^4I_{15/2}$ and $^4F_{9/2}$ → $^4I_{15/2}$ transitions were identical to those published previously on single-crystal GGG:Er^{3+}.[19] Furthermore, NIR emission was observed from the $^4I_{9/2}$ → $^4I_{15/2}$ transition between 780 and 820 nm and from the $^4S_{3/2}$ → $^4I_{13/2}$ transition between 830 and 870 nm (Figure 2, inset). Similarly, NIR emission was also observed between 900 and 1075 nm and from 1400 to 1700 nm ascribed to the transitions from the $^4I_{11/2}$ and $^4I_{13/2}$ excited states to the $^4I_{15/2}$ ground state as well as a very weak emission from the $^4S_{3/2}$ → $^4I_{11/2}$ transition between 1225 and 1275 nm (Figure 3). As can be seen from Figures 2 and 3, the overall Stark structures of the emission bands in the 1 and 5% samples are identical.

In previous studies on Er^{3+}-doped nanocrystalline cubic sesquioxides (Y_2O_3 and Lu_2O_3) prepared using a similar synthesis procedure, we showed that the medium infrared (MIR) spectra of the nanocrystals contained intense bands centered around 1500 and 3350 cm^{-1}, which were assigned to vibrations from the CO_3^{2-} and OH^- species present on the particle surface.[27−29] The emission intensity from the ($^2H_{11/2}$, $^4S_{3/2}$) → $^4I_{15/2}$ and $^4F_{9/2}$ → $^4I_{15/2}$ transitions in the nanocrystalline material

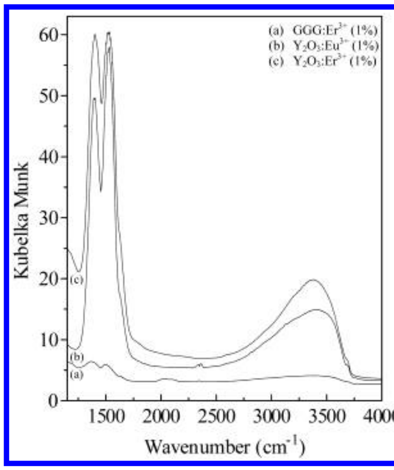

Figure 4. Medium-infrared (MIR) reflectance spectra of nanocrystalline (a) GGG:Er 1%, (b) Y_2O_3:Eu 1%, and (c) Y_2O_3:Er 1%.

TABLE 1: Decay Times of Nanocrystalline GGG:Er^{3+} Following Excitation with 488 nm. In the Case of the 5% Doped Sample, the Values of the Decay Time Constant τ_m Are Reported

	nanocrystalline $Gd_3Ga_5O_{12}:Er^{3+}$ decay times (μs)	
transition	1% Er^{3+}	5% Er^{3+}
$^2H_{11/2}$ → $^4I_{15/2}$	122	89
$^4S_{3/2}$ → $^4I_{15/2}$	123	81
$^4F_{9/2}$ → $^4I_{15/2}$	117	58
$^4S_{3/2}$ → $^4I_{13/2}$	113	81

was significantly lower than the bulk material, where no bands were observed in the MIR spectra. The reduction in intensity was attributed to an increase in the nonradiative decay from the emitting states as it is well-known that an increase in the effective phonon energy of the material will have the resultant effect of increasing the rate of multiphonon relaxation (W_{MPR}).[30] Interestingly enough as can be seen from Figure 4, the MIR spectrum of nanocrystalline $Gd_3Ga_5O_{12}:Er^{3+}$ shows that the bands at 1500 and 3350 cm^{-1} are significantly reduced compared to the Eu^{3+}- and Er^{3+}-doped Y_2O_3 nanocrystals, for example. This has the desired effect of considerably increasing the luminescence efficiency of nanocrystalline GGG:Er^{3+} in comparison to either $Y_2O_3:Er^{3+}$ or $Lu_2O_3:Er^{3+}$ nanocrystals.

The decay times following excitation with 488 nm, are presented in Table 1. The decay curves for the 1% nanocrystalline GGG:Er^{3+} were exponential and thus could be fitted with a single-exponential model. However, when the concentration of Er^{3+} was increased to 5%, the decay curves deviated from single exponentiality. At low erbium ion concentrations, the $Er^{3+}-Er^{3+}$ interactions are negligible and, as a result, the decay curves will be exponential. At higher Er^{3+} concentrations, the ion−ion interactions increase and thus the interactions between dopant ions become more prominent. These ion−ion interactions causes the observed deviation from exponentiality in the 5% GGG:Er^{3+} sample and the degree of nonexponentiality increases with increasing dopant concentration. Therefore, fitting the decay curves of the 5% sample with a single-exponential function was no longer a valid option. We determined the emission decay time constant, τ_m, using the following equation:[31]

$$\tau_m = \frac{\int_0^\infty tI(t)\,dt}{\int_0^\infty I(t)\,dt} \tag{1}$$

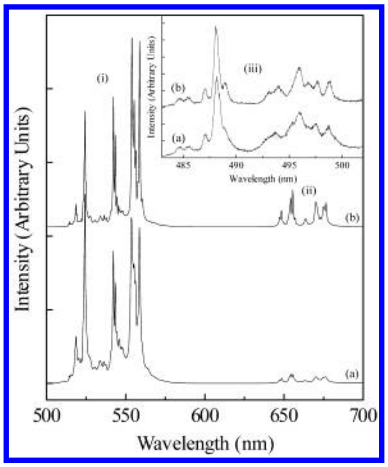

Figure 5. Upconversion spectrum of nanocrystalline GGG:Er^{3+} doped with (a) 1% and (b) 5% Er^{3+} following excitation with 800 nm and showing the following transitions: (i) ($^2H_{11/2}$, $^4S_{3/2}$) $\rightarrow$ $^4I_{15/2}$, (ii) $^4F_{9/2}$ $\rightarrow$ $^4I_{15/2}$. Inset: (iii) $^4F_{7/2}$ $\rightarrow$ $^4I_{15/2}$.

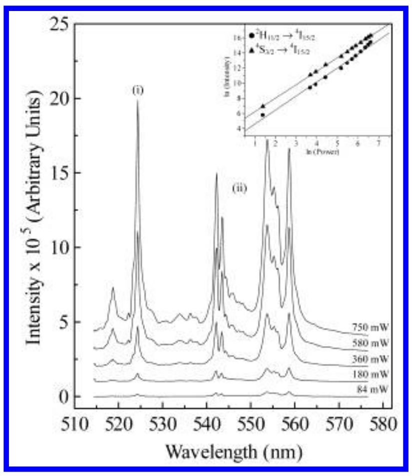

Figure 6. Power dependence of the upconverted (i) $^2H_{11/2}$ $\rightarrow$ $^4I_{15/2}$ and (ii) $^4S_{3/2}$ $\rightarrow$ $^4I_{15/2}$ emission in nanocrystalline GGG:Er^{3+}-doped 1% Er^{3+} following excitation with 800 nm. Inset: Graph of ln(I_i) versus ln(I_o) yielding slopes of approximately 2 for both transitions.

where: $I(t)$ is the intensity at time t. As seen from Table 1, the decay times for the more heavily doped sample are considerably shorter in comparison to the more weakly doped sample. In the 5% sample the dynamics become influenced by the aforementioned energy transfer processes which make the decay time shorter.[32]

Following excitation of the $^4I_{9/2}$ $\leftarrow$ $^4I_{15/2}$ transition using 800 nm radiation, intense upconverted emission was observed in both 1 and 5% nanocrystalline GGG:Er^{3+} samples (Figure 5). Green emission from the thermalized ($^2H_{11/2}$, $^4S_{3/2}$) $\rightarrow$ $^4I_{15/2}$ transition and red emission from the $^4F_{9/2}$ $\rightarrow$ $^4I_{15/2}$ transition were observed centered at approximately 540 and 660 nm, respectively. Similarly, a relatively weak blue emission assigned to the transition from the $^4F_{7/2}$ excited state to the $^4I_{15/2}$ ground state was observed centered at approximately 492 nm (Figure 5, inset). It is worth mentioning that the visually dominant green emission was still observed when pumping with < 5 mW of excitation power.

To obtain a better understanding of the process of upconversion, a power dependence study of the upconverted emission intensity was performed (Figure 6). It has been shown that the intensity of the upconverted emission, I_o, is proportional to some

TABLE 2: Decay Times of Nanocrystalline GGG:Er^{3+} Following Excitation with 800 nm. In the Case of the 5% Doped Sample, the Values of the Decay Time Constant τ_m Are Reported

	nanocrystalline $Gd_3Ga_5O_{12}$:Er^{3+} Decay Times (μs)	
transition	1% Er^{3+}	5% Er^{3+}
$^2H_{11/2} \rightarrow {}^4I_{15/2}$	119	172
$^4S_{3/2} \rightarrow {}^4I_{15/2}$	123	167
$^4F_{9/2} \rightarrow {}^4I_{15/2}$	117	830

power n of the NIR excitation intensity, I_i, and can be written as follows:[33]

$$I_o \propto I_i^n \qquad (2)$$

where $n = 1, 2, 3, ...$, etc. The superscript n is the number of photons required to populate the emitting state and was determined from the slope of the graph, ln (I_i) versus ln (I_o). Thus, fitting the data to a straight line yielded slopes of approximately 2 for the ($^2H_{11/2}$, $^4S_{3/2}$) $\rightarrow$ $^4I_{15/2}$ and $^4F_{9/2}$ $\rightarrow$ $^4I_{15/2}$ transitions for both 1 and 5% GGG:Er^{3+} nanocrystal samples (Figure 6, inset) therefore indicating that the upconversion process was achieved via a two-photon process. There are essentially three main mechanisms of upconversion. Excited state absorption (ESA) involves only a single ion, and thus it is usually the only upconversion process which occurs in materials with low dopant concentrations.[34] In this process, an incoming photon from the pump beam will bring the ion to an intermediate excited level and a second photon will proceed to bring the ion to the upper emitting level. The upconverted luminescence intensity in this process usually varies quadratically with the pump beam but varies linearly with the concentration of the rare-earth dopant.[35] Energy transfer upconversion (ETU) involves two ions in close proximity, which are excited by the pump beam to an intermediate level. The two ions are coupled by a nonradiative process in which one relaxes to a lower lying state, while the other ion is promoted to the upper emitting level.[36] Much like ESA, the population of the upper emitting level in the ETU process varies quadratically with the density of photons in the pump beam. However, ETU differs from ESA in that the upconversion luminescence also varies quadratically with the dopant concentration. Finally, photon avalanche (PA) upconversion is produced by absorption from an excited state of the rare-earth ion where the pump laser wavelength is resonant with a transition from this intermediate metastable level to the upper emitting state. Therefore, an energy transfer process is responsible for producing the population in the intermediate excited state.[37] In PA, one ion initially in the intermediate level produces two ions in this state as a result of photon absorption and subsequent energy transfer. Under the right pumping conditions, two ions can produce four in the intermediate state, four can produce eight, the eight can produce sixteen, etc. The PA process requires a minimum pump intensity and is characterized by a pump threshold, which if not achieved will result in inefficient upconversion.[38]

It was established by the power-dependence study of the anti-Stokes emission that the upconversion occurred via a two-photon process. Since no inflection point was observed in the graph of ln (I_i) versus ln (I_o), PA was discounted as a mechanism of upconversion thus indicating that it could occur via ESA or ETU mechanisms. Table 2 presents the decay times of $Gd_3Ga_5O_{12}$:Er^{3+} (1 and 5%) following excitation with 800 nm. As with the decay times obtained following 488 nm excitation, the upconverted decay curves of the 5% sample deviated from

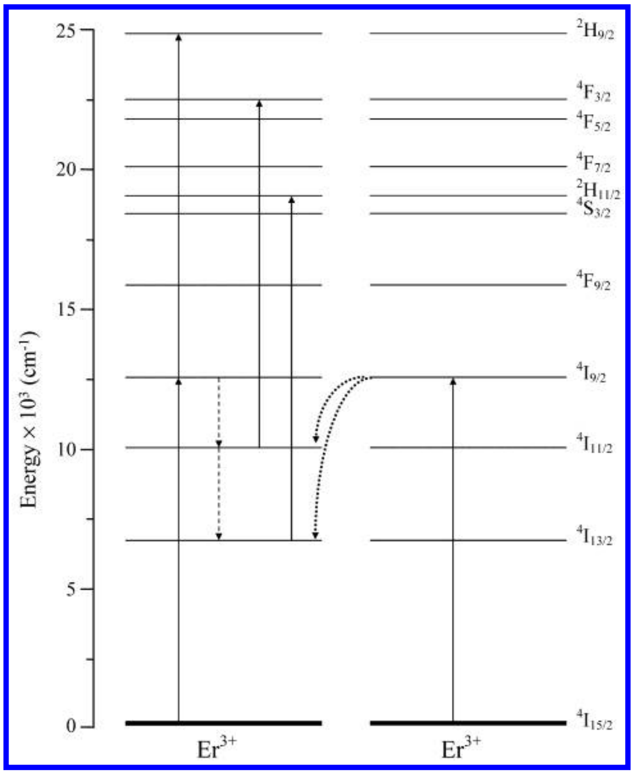

Figure 7. Diagram showing the excited-state absorption (ESA) and energy transfer upconversion (ETU) mechanisms in nanocrystalline GGG:Er^{3+} following excitation with 800 nm into the $^4I_{9/2}$ state.

exponentiality. It is worth mentioning that the decay times in the 1% sample were identical at both pumping wavelengths. However in the 5% sample, the decay times obtained following excitation with 800 nm were lengthened compared to those obtained following direct excitation ($\lambda_{exc} = 488$ nm). This decay lengthening is a clear indication of the presence of ETU.[21]

From the upconversion decay times, it is clear that excited-state absorption is the dominant mechanism in the nanocrystalline 1% GGG:Er^{3+} sample (Figure 7). In this process, an 800 nm photon from the pump beam excites the ion to the $^4I_{9/2}$ excited state. However, rapid multiphonon relaxation from $^4I_{9/2}$ to $^4I_{11/2}$ is a property common to all fluorides and oxides,[39,40] and thus the resonant $^2H_{9/2} \leftarrow {}^4I_{9/2}$ transition, which occurs following absorption of a second photon, is not the most probable, forcing us to consider alternate upconversion pathways. Therefore, once the ion is excited to the $^4I_{9/2}$ intermediate level, it will nonradiatively decay to the $^4I_{11/2}$ state. A second photon from the pump beam will then excite the Er^{3+} ion to the $^4F_{3/2}$ state. Nonradiative relaxation, in turn, populates the lower emitting states. Alternately, the ion can decay nonradiatively to the $^4I_{13/2}$ state and a second 800 nm photon will populate the $^2H_{11/2}$ state. The upconverted emission is then observed from this and the lower emitting states.

As evidenced by the decay time lengthening following excitation with 800 nm, energy transfer upconversion becomes more efficient and thus is presumably the dominant mechanism in the 5% nanocrystalline sample (Figure 7). In this process, two Er^{3+} ions in close proximity are excited to the $^4I_{9/2}$ intermediate state following absorption of 800 nm radiation. One Er^{3+} ion nonradiatively decays to the $^4I_{11/2}$ state and is excited to the $^4F_{3/2}$ state via the transfer of energy from the neighboring Er^{3+} ion in the $^4I_{9/2}$ state, which then returns to the $^4I_{15/2}$ ground state. Alternatively, the initial ion can decay to the $^4I_{13/2}$ state, and following energy transfer from another ion in the $^4I_{9/2}$ state, the $^2H_{11/2}$ level is populated. Upconverted emission is subsequently observed from this and the lower lying excited states.

We notice from the upconversion spectra, which are normalized to the green ($^2H_{11/2}$, $^4S_{3/2} \rightarrow {}^4I_{15/2}$) transition, that the red ($^4F_{9/2} \rightarrow {}^4I_{15/2}$) transition is more intense in the 5% nanocrystalline GGG:Er^{3+} sample. If the ESA and ETU mechanisms described earlier are the only processes operative, we would expect the green ($^2H_{11/2}$, $^4S_{3/2}$) $\rightarrow {}^4I_{15/2}$ and red $^4F_{9/2} \rightarrow {}^4I_{15/2}$ transitions in the upconversion spectrum to have identical relative intensities as in the direct emission ($\lambda_{exc} = 488$ nm) spectrum. However, this is not the case as the intensity of the $^4F_{9/2} \rightarrow {}^4I_{15/2}$ transition grows at a more rapid rate than the green ($^2H_{11/2}$, $^4S_{3/2}$) $\rightarrow {}^4I_{15/2}$ transition. In a previous paper,[28] we similarly observed an enhancement of the red $^4F_{9/2} \rightarrow {}^4I_{15/2}$ emission in $Y_2O_3:Er^{3+}$ nanocrystals (1, 2, 5, and 10 mol %) synthesized by identical techniques. Following excitation at 815 nm, the upconverted luminescence in the 1 mol % $Y_2O_3:Er^{3+}$ was very weak in comparison to the 10 mol % nanocrystal sample. However, as the dopant Er^{3+} concentration was increased to 10 mol %, the upconversion became more intense with emission from the red ($^4F_{9/2} \rightarrow {}^4I_{15/2}$) transition increasing at a more rapid rate than that from the green ($^2H_{11/2}$, $^4S_{3/2} \rightarrow {}^4I_{15/2}$) transition. In the 10 mol % doped sample, the intensity of the red emission became more intense than that of the green emission. Furthermore, Chen et al. [19] studied the upconversion properties of single-crystal $Gd_3Ga_5O_{12}$ doped with 1, 10, and 30% Er^{3+} following excitation with 790 nm from a semiconductor diode. They observed that when the GGG:Er^{3+} single crystals were pumped with 790 nm, both the green and red upconverted emission became much more intense with increasing concentration of erbium ions. However, they also observed that the red emission became stronger by a greater factor than the green emission. Thus, it was postulated that a second mechanism was responsible for populating the $^4F_{9/2}$ level only. In 5% nanocrystalline $Gd_3Ga_5O_{12}:Er^{3+}$, it is therefore probable that an additional mechanism is operative, which directly populates the $^4F_{9/2}$ state. In this mechanism, 800 nm photons excite two neighboring ions in close proximity to the $^4I_{9/2}$ level, followed by the quick nonradiative decay of one of the ions to the $^4I_{11/2}$ state. Since the energy gap from this state to the $^4F_{9/2}$ level is identical to the gap from the intermediate $^4I_{9/2}$ state to the $^4I_{13/2}$ level, the two ions undergo an ion-pair process of the type ($^4I_{9/2}$, $^4I_{11/2}$) $\rightarrow$ ($^4I_{13/2}$, $^4F_{9/2}$). This additional upconversion mechanism is wholly responsible for populating the $^4F_{9/2}$ level and results in the observed phenomenon of $^4F_{9/2} \rightarrow {}^4I_{15/2}$ emission enhancement (Figure 8). Moreover, the upconverted decay time of the $^4F_{9/2}$ excited state in the 5% nanocrystal sample is severely lengthened compared to the decay obtained with 488 nm excitation (830 μs compared to 58 μs). This is indicative of the presence of a very efficient energy transfer process and clearly illustrates that the mechanism responsible for the enhancement of the red emission is a highly concentration-dependent process. Clearly, further experiments are required to fully probe the phenomenon of the red emission enhancement in these materials. Dynamical studies utilizing pulsed excitation wavelengths have been initiated and will be the subject of a future paper.

4. Conclusions

In this paper, we demonstrated for the first time near-infrared to visible upconversion in nanocrystalline $Gd_3Ga_5O_{12}$ doped with Er^{3+} ions. Green emission from the ($^2H_{11/2}$, $^4S_{3/2}$) $\rightarrow {}^4I_{15/2}$ and red emission from the $^4F_{9/2} \rightarrow {}^4I_{15/2}$ transitions were observed following excitation with 800 nm into the $^4I_{9/2}$ state. Nanocrystalline samples of GGG:Er^{3+} with 1 and 5% Er^{3+} dopant

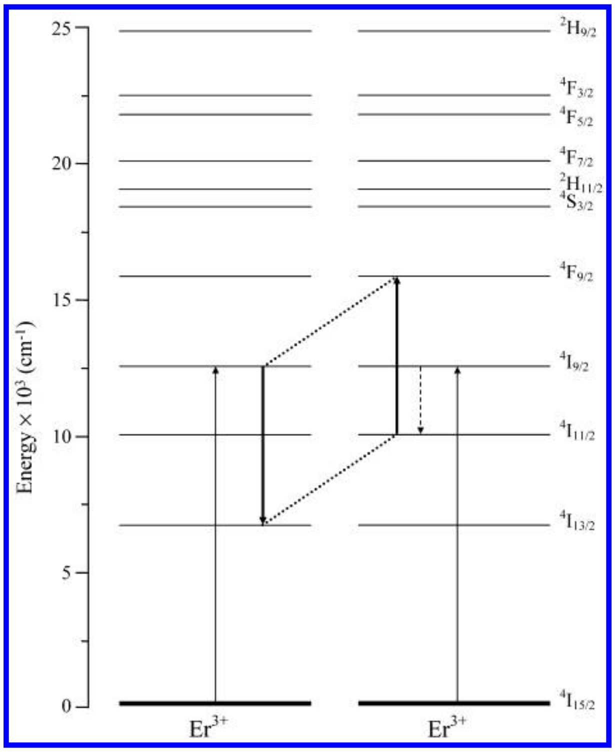

Figure 8. Diagram showing the ($^4I_{9/2}$, $^4I_{11/2}$) → ($^4I_{13/2}$, $^4F_{9/2}$) ion pair process responsible only for $^4F_{9/2}$ state

concentrations were studied and it was determined that upconversion occurred via excited-state absorption in the 1% sample while energy transfer upconversion took over as the dominant mechanism as the concentration was increased to 5% as evidenced from the lengthening of the upconverted decay times. Furthermore, an enhancement of the red ($^4F_{9/2} \rightarrow {}^4I_{15/2}$) emission was observed and hypothesized to occur via the concentration-dependent ($^4I_{9/2}$, $^4I_{11/2}$) → ($^4I_{13/2}$, $^4F_{9/2}$) ion pair process, which directly populated the $^4F_{9/2}$ state.

Acknowledgment. The authors gratefully thank Erica Viviani (Università di Verona, Italy) for expert technical assistance and Stefano Polizzi (Università di Venezia, Italy) for the X-ray measurements on nanocrystalline $Gd_3Ga_5O_{12}$:Er^{3+}. The authors acknowledge the Natural Science and Engineering Research Council of Canada and MURST (project 9903222581_005) of Italy, for financial support.

References and Notes

(1) Tissue, B. M. *Chem. Mater.* **1998**, *10*, 2837−2845.
(2) Williams, D. K.; Yuan, H.; Tissue, B. M. *J. Lumin.* **1999**, *83−84*, 297−300.
(3) Huignard, A.; Gacoin, T.; Boilot, J.-P. *Chem. Mater.* **2000**, *12*, 1090−1094.
(4) Riwotzki, K.; Hasse, M. *J. Phys. Chem. B* **1998**, *102*, 10129−10135.
(5) Zhang, H. X.; Kam, C. H.; Zhou, Y.; Han, X. Q.; Buddhudu, S.; Lam, Y. L. *Opt. Mater.* **2000**, *15*, 47−50.
(6) Yi, G.; Sun, B.; Yang, F.; Chen, D.; Zhou, Y.; Cheng, J. *Chem. Mater.* **2002**, *14*, 2910−2914.
(7) Bender, C. M.; Burlitch, J. M.; Barber, D.; Pollock, C. *Chem. Mater.* **2000**, *12*, 1969−1976.
(8) Shea, L. E.; McKittrick, J.; Lopez, O. A. *J. Am. Ceram. Soc.* **1996**, *79*, 3257−3265.
(9) McKittrick, J.; Shea, L. E.; Bacalski, C. F.; Bosze, E. J. *Displays* **1999**, *19*, 169−172.
(10) Hreniak, D.; Strek, W. *J. Alloy Compd.* **2002**, *341*, 183−186.
(11) Lu, C.-H.; Hong, H.-C.; Jagannathan, R. *J. Mater. Sci. Lett.* **2002**, *21*, 1489−1492.
(12) Lenth, W.; Macfarlane, R. M. In *Opt. Photon. News* 1992; Vol. 3, p 8−15.
(13) Scheps, R. *Prog. Quantum Electron.* **1996**, *20*, 271−358.
(14) Lupei, V. *Opt. Mater.* **2002**, *19*, 95−107.
(15) Sugak, D.; Matkovskii, A.; Durygin, A.; Suchocki, A.; Solskii, I.; Ubizskii, S.; Kopczynski, K.; Mierczyk, Z.; Potera, P. *J. Lumin.* **1999**, *82*.
(16) Gill, D. S.; Anderson, A. A.; Eason, R. W.; Warburton, T. J.; Shepherd, D. P. *Appl. Phys. Lett.* **1996**, *69*, 10−12.
(17) Dong, J.; Lu, K. *Phys. Rev. B* **1991**, *43*, 8808−8821.
(18) Xu, Y.-N.; Ching, W. Y.; Brickeen, B. K. *Phys. Rev. B* **2000**, *61*, 1817−1824.
(19) Chen, X.; Nguyen, T.; Luu, Q.; Di Bartolo, B. *J. Lumin.* **2000**, *85*, 295−299.
(20) Lundt, H.; Weidner, H. *Opt. Commun.* **1991**, *82*, 484−487.
(21) Capobianco, J. A.; Raspa, N.; Monteil, A.; Malinowski, M. *J. Phys.: Condens. Matter* **1993**, *5*, 6083−6090.
(22) Kir'yanov, A. V.; Aboites, V.; Belovolov, A. M.; Timoshechkin, M. I.; Belovolov, M. I.; Damzen, M. J.; Minassian, A. *Opt. Express* **2002**, *10*, 832−839.
(23) Wyss, C. P.; Kehrli, M.; Huber, T.; Morris, P. J.; Lüthy, W.; Weber, H. P.; Zagumennyi, A. I.; Zavartsev, Y. D.; Studenikin, P. A.; Shcherbakov, I. A.; Zerrouk, A. F. *J. Lumin.* **1999**, *82*, 137−144.
(24) Tao, Y.; Zhao, G.; Zhang, W.; Xia, S. *Mater. Res. Bull.* **1997**, *32*, 501−506.
(25) Tessari, G.; Bettinelli, M.; Speghini, A.; Ajò, D.; Pozza, G.; Depero, L. E.; Allieri, B.; Sangaletti, L. *Appl. Surf. Sci.* **1999**, *144−145*, 686−689.
(26) Polizzi, S. Unpublished results.
(27) Capobianco, J. A.; Vetrone, F.; D'Alesio, T.; Tessari, G.; Speghini, A.; Bettinelli, M. *Phys. Chem. Chem. Phys.* **2000**, *2*, 3203−3207.
(28) Capobianco, J. A.; Vetrone, F.; Boyer, J. C.; Speghini, A.; Bettinelli, M. *J. Phys. Chem. B* **2002**, *106*, 1181−1187.
(29) Capobianco, J. A.; Vetrone, F.; Boyer, J. C.; Speghini, A.; Bettinelli, M. *Opt. Mater.* **2002**, *19*, 259−268.
(30) Riseberg, L. A.; Moos, H. W. *Phys. Rev.* **1968**, *174*, 429−438.
(31) Nakazawa, E. In *Phosphor Handbook*; Shionoya, S., Yen, W. M., Eds.; CRC Press: Boca Raton, FL, 1999.
(32) Capobianco, J. A.; Kabro, P.; Ermeneux, F. S.; Moncorgé, R.; Bettinelli, M.; Cavalli, E. *J. Appl. Phys.* **1997**, *82*, 3983−3986.
(33) Pollnau, M.; Gamelin, D. R.; Lüthi, S. R.; Güdel, H. U.; Hehlen, M. P. *Phys. Rev. B* **2000**, *61*, 3337−3346.
(34) Bloembergen, N. *Phys. Rev. Lett.* **1959**, *2*, 84−85.
(35) Vetrone, F.; Boyer, J. C.; Capobianco, J. A.; Speghini, A.; Bettinelli, M. *J. Phys. Chem. B* **2002**, *106*, 5622−5628.
(36) Auzel, F. *C. R. Acad. Sci. (Paris)* **1966**, *262*, 1016−1019.
(37) Chivian, J. S.; Case, W. E.; Eden, D. D. *Appl. Phys. Lett.* **1979**, *35*, 124−125.
(38) Joubert, M. F.; Guy, S.; Jacquier, B. *Phys. Rev. B* **1993**, *48*, 10031−10037.
(39) Weber, T.; Lüthy, W.; Weber, H. P. *Appl. Phys. B* **1992**, *B55*, 144−148.
(40) Lüthi, S. R.; Pollnau, M.; Güdel, H. U. *Phys. Rev. B* **1999**, *60*, 162−178.